

1 Supplementary information for manuscript

2
3 **Spatial variation of chemical composition and sources of submicron aerosol in**
4 **Zurich during wintertime using mobile aerosol mass spectrometer data**

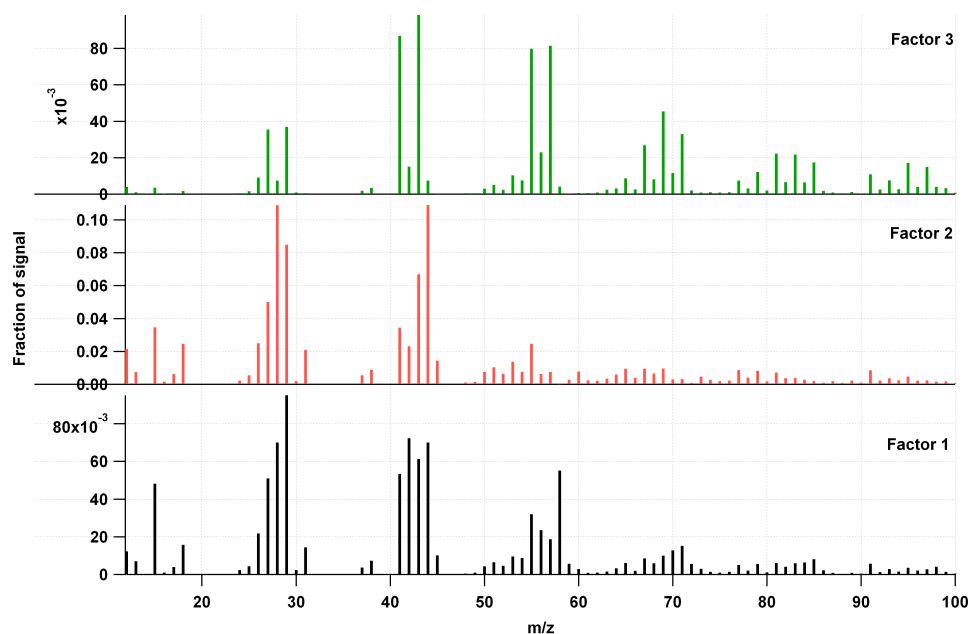
5
6 **C. Mohr¹, R. Richter¹, Peter F. DeCarlo^{1,*}, A. S. H. Prévôt¹, U. Baltensperger¹**

7 ¹ Laboratory of Atmospheric Chemistry, Paul Scherrer Institut (PSI), Villigen, Switzerland

8 * now an AAAS Science and Technology Policy Fellow hosted at the US EPA, Washington DC,
9 USA

10
11 Correspondence to: A. S. H. Prévôt (andre.prevot@psi.ch)

12
13 **1 Preparatory data analysis**



14
15 **Figure SI- 1: 3-factorial solution of running the PMF2 algorithm on the organic data matrix where the m/z 's**
16 **directly proportional to m/z 44 were downweighted.**

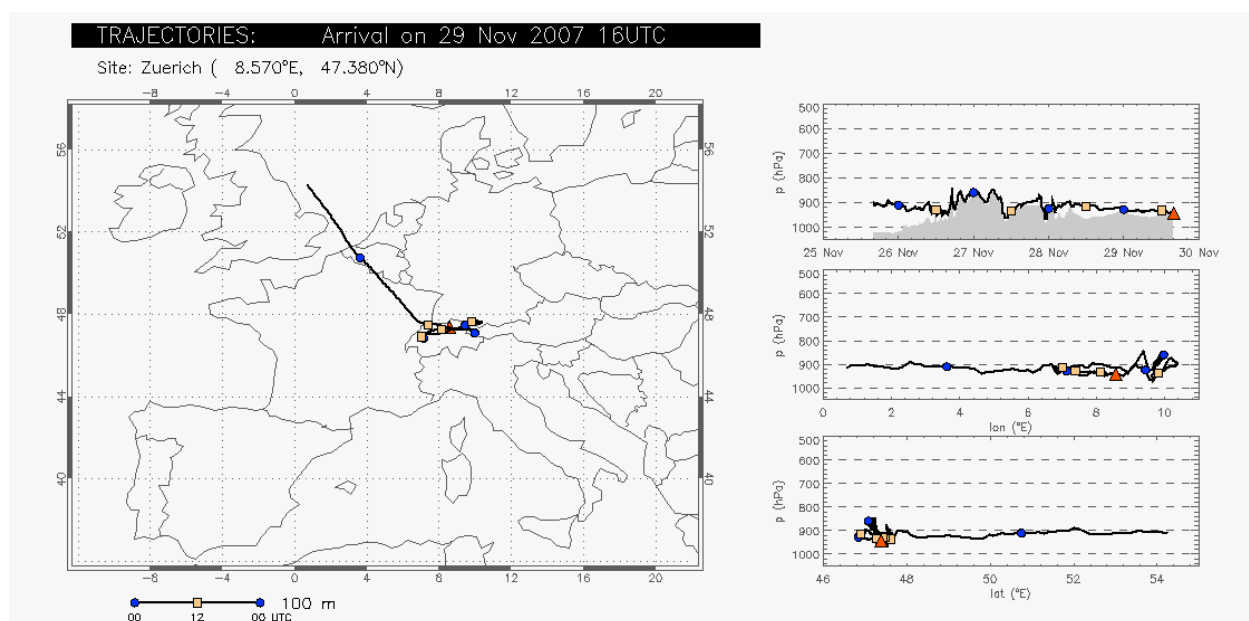
17
18 When downweighting m/z 's directly proportional to m/z 44, the PMF solution does not fully
19 separate OOA and WBOA. m/z 's 60 and 73, markers for BBOA (Alfarra et al., 2007), show up

20 in Factor 2, which resembles OOA with the dominating signal at m/z 44 (see also section 3.2 in
21 the manuscript). As for the corresponding time series (not shown), both Factor 1 and Factor 2
22 follow periodically the time series of inorganic secondary components, but no consistent
23 comparison can be done.

24 2 Air mass back trajectories

25 Four-day backward trajectories were calculated based on 3-dimensional wind fields of the
26 regional weather prediction model COSMO using the trajectory model TRAJ (Fay et al., 1995).
27 The fields were taken from hourly "analyses" operationally generated by the Swiss weather
28 service MeteoSwiss at a resolution of 7 km x 7 km x 60 vertical levels for a domain covering
29 large parts of Europe.

30

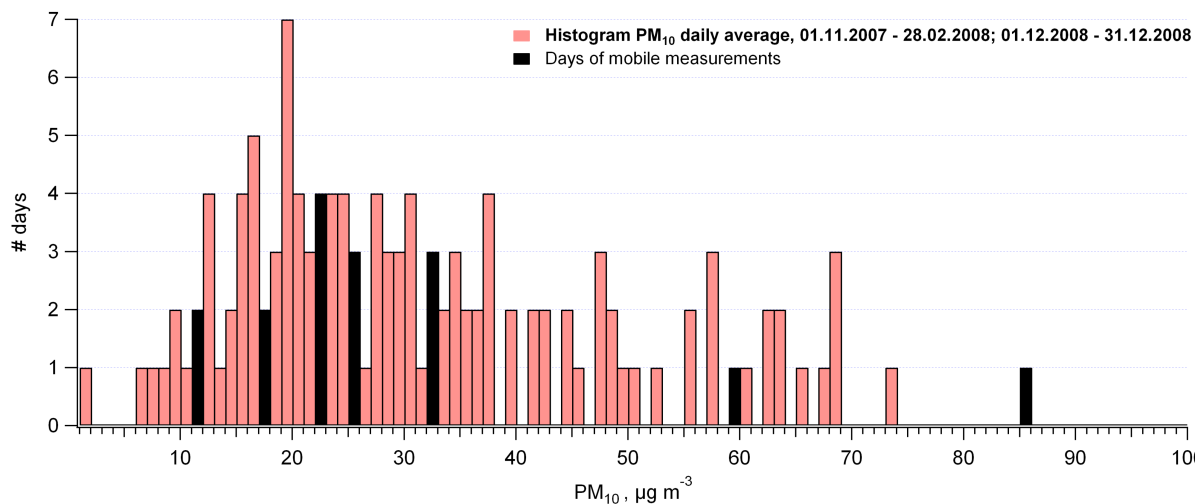


32 **Figure SI- 2: Air mass back trajectories for 29 November 2007. Air masses moved from Belgium/Germany to**
33 **Switzerland and stagnated over the Swiss plateau, residing there for about 3 days prior to reaching the**
34 **receptor site Zurich Kaserne (red triangle).**

35

36

37 **3 Representativeness plot of mobile measurements**

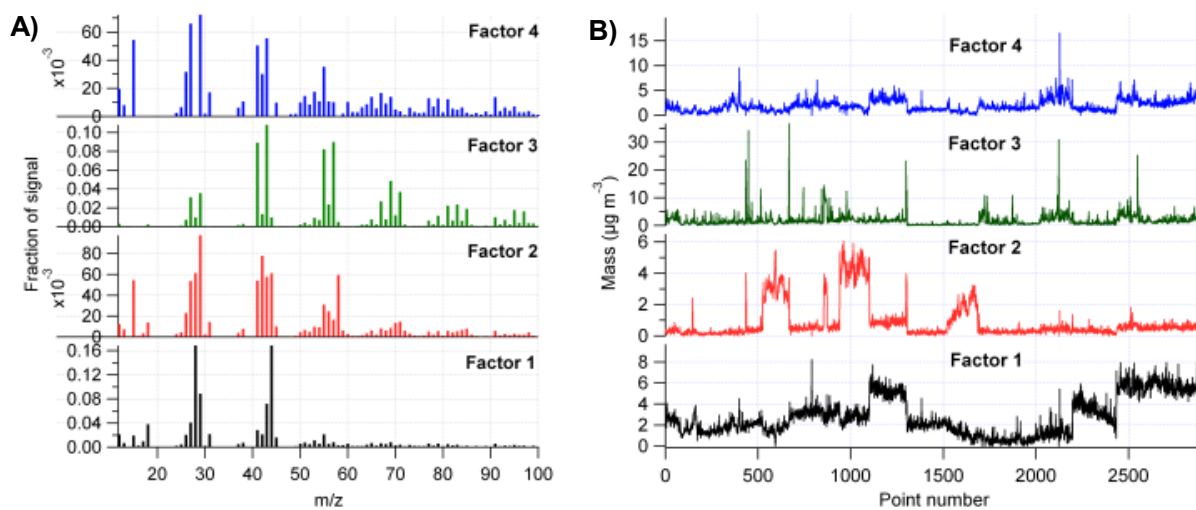


38
39 **Figure SI- 3: Histogram of PM₁₀ daily mean values for the periods of 01 November 2007 – 31 February 2008**
40 **and 01 December 2008 – 31 December 2008. Values of days when mobile measurements were performed are**
41 **colored in black.**

42

43 **4 PMF diagnostics**

44



45
46 **Figure SI- 4: 4-factor solution for part 1, source spectra (F, panel A), and time series (G, panel B).**

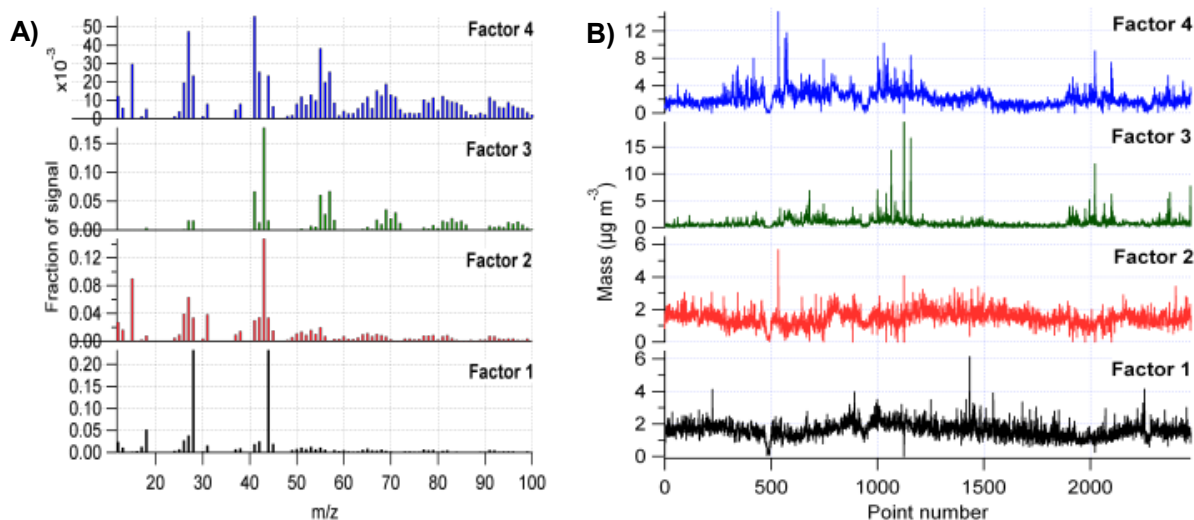
47

48 Choosing $p > 3$ did not yield meaningful results. For part 1, $p \geq 4$ resulted in an additional factor
49 similar to BBOA and OOA and a prominent peak at m/z 58 related to amines, most likely an

50 artifact of inlet contamination during overnight parking of the mobile laboratory at a garage of
51 public transport buses. This amine factor was persistent also for an increasing number of p with
52 no meaningful factors. Adding an additional factor for part 2 led to a split of the HOA factor
53 (Fig. SI-5), with 2 factors featuring high signal at m/z 43.

54 For part 1, $p = 4$, the resulting additional factor 2 (Fig. SI-4) shows high similarity with factor 1
55 (Pearson's $R = 0.74$) and factor 4 (Pearson's $R = 0.77$) and can be interpreted as a recombination
56 of OOA and BBOA. Interestingly, it features a few distinct peaks relating to the ion series
57 ($C_nH_{2n+2}N$) characteristic for amines, e. g. m/z 58 (Silva et al., 2008). As shown by the time
58 series of factor 2 in panel B), there were 3 measurement drives with substantial factor 2 mass
59 loadings – drives following a night when the mobile laboratory had been parked in a garage of
60 public transport buses in Zurich. The punctual occurrence of this factor and the missing
61 analogies in volatile organic compounds (VOC) time series measured at Zurich Kaserne (not
62 shown) lead to the hypothesis that the amine signal could be explained by emissions related to
63 SCR (selective catalytic reduction, a NO_x abatement technology using an aqueous urea solution
64 (Koebel et al., 2000)) systems the buses are equipped with to meet the EURO V legal emission
65 standards (implemented in Switzerland on 1 September 2009).

66 Running PMF excluding the amine-influenced periods yielded the same 3 factors as for the
67 complete part 1 dataset ($R^2 > 0.99$ for all 3 factors). The 3-factorial solution of the full part 1
68 dataset exhibits elevated total residual masses for those 3 measurement drives (Fig. SI-13),
69 mostly due to m/z 58 (compare non-normally distributed scaled residuals for m/z 58 in the inset
70 of Fig. SI-14).



71

72 **Figure SI- 5: 4-factor solution for part 2, source spectra (F, panel A), and time series (G, panel B).**

73

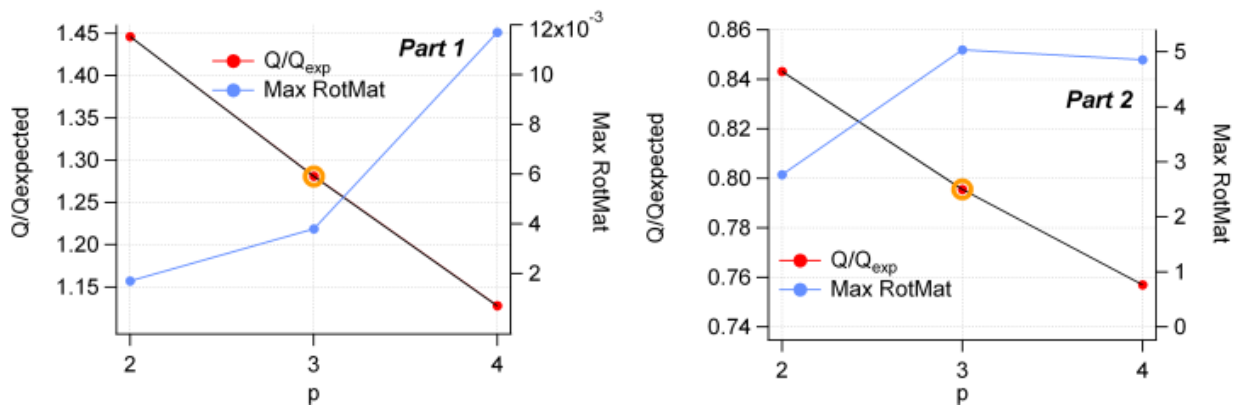
74 The Q -value is one mathematical criterion for the quality of the fit (compare Eq. 2 in main
 75 paper). If the model is appropriate for the problem at hand and the data uncertainties estimations
 76 are accurate, then $(e_{ij} / \sigma_{ij})^2$ is ~ 1 and the expected Q (Q_{exp}) = $mn - p(m+n) \approx mn$, the degrees of
 77 freedom of the fitted data. $Q/Q_{exp} \gg 1$ indicates an underestimation, $Q/Q_{exp} \ll 1$ an
 78 overestimation of errors in the input data (Paatero et al., 2002). Each added factor introduces
 79 more degrees of freedom allowing more data to be fit and hence decreases Q . From a
 80 mathematical point of view, the correct value of p in PMF is where the line changes the slope in
 81 the plot of a series of p values versus their respective minimized Q . However, PMF solutions of
 82 ambient datasets also have to be feasible in an ambient context and hence it is the subjective task
 83 of the modeler to choose a set of factors able to explain real world phenomena which may or
 84 may not correspond to the mathematically correct value of p .

85 Another parameter to explore the quality of the PMF fit is $max(rotmat)$, the largest element in
 86 **RotMat** where PMF2 reports the standard deviation of possible values of the transformation
 87 matrix **T**. PMF solutions are not unique since linear transformation still conserving the non-
 88 negativity constraint may be possible ($\mathbf{GF} = \mathbf{GTT}^{-1}\mathbf{F}$). This rotational indeterminacy is a
 89 significant problem in the use of factor analysis (Paatero et al., 2002). Generally, the best fit
 90 demands a minimal $max(rotmat)$, since larger values in **T** imply greater rotational freedom of a
 91 solution. However, it has been stated clearly (e. g. Lanz et al., 2007) that “**RotMat** values [...]”
 92 are not suited as a unique criterion for the determination of the number of factors” (compare

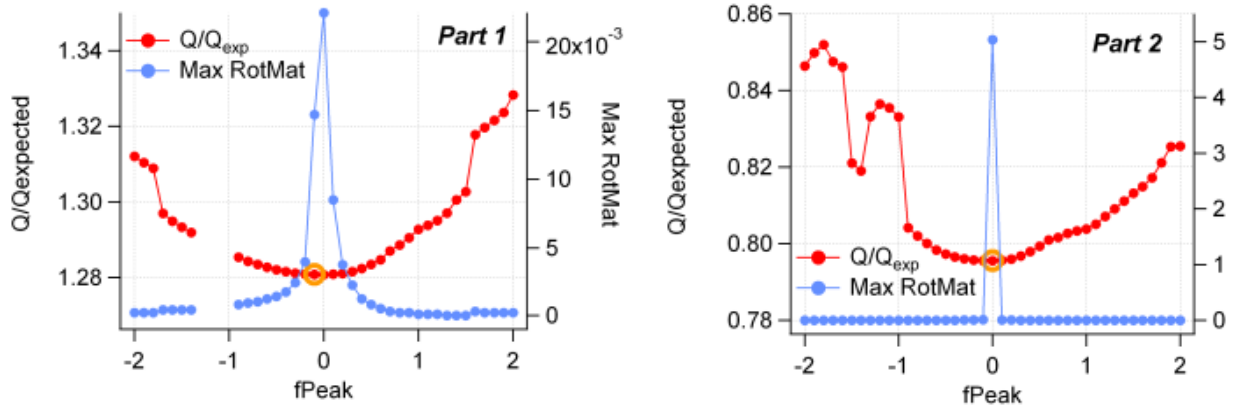
93 Figure SI-6, right panel: For part 2, a solution purely based on $\max(\text{rotmat})$ would not include
94 $p = 3$).

95 Once p has been defined, the rotational freedom of the chosen solution may be explored through
96 a non-zero valued user-specified rotational parameter f_{peak} . $f_{\text{peak}} > 0$ tries to impose rotations
97 on the emerging solutions using positive coefficients r in \mathbf{T} , $f_{\text{peak}} < 0$ vice versa. $f_{\text{peak}} = 0$
98 produces the most central solution. f_{peak} was chosen to be -0.1 for part 1, and 0 for part 2, based
99 on a trade-off between “high” signal at m/z 60 ($\text{C}_2\text{H}_4\text{O}_2^+$, among others a fragment of
100 levoglucosan which in turn is a pyrolysis product of cellulose and hence a marker of biomass
101 burning emissions (Alfarra et al., 2007)), and non-zero signal at m/z 44 (predominantly non-
102 gaseous CO_2^+) in the BBOA spectrum.

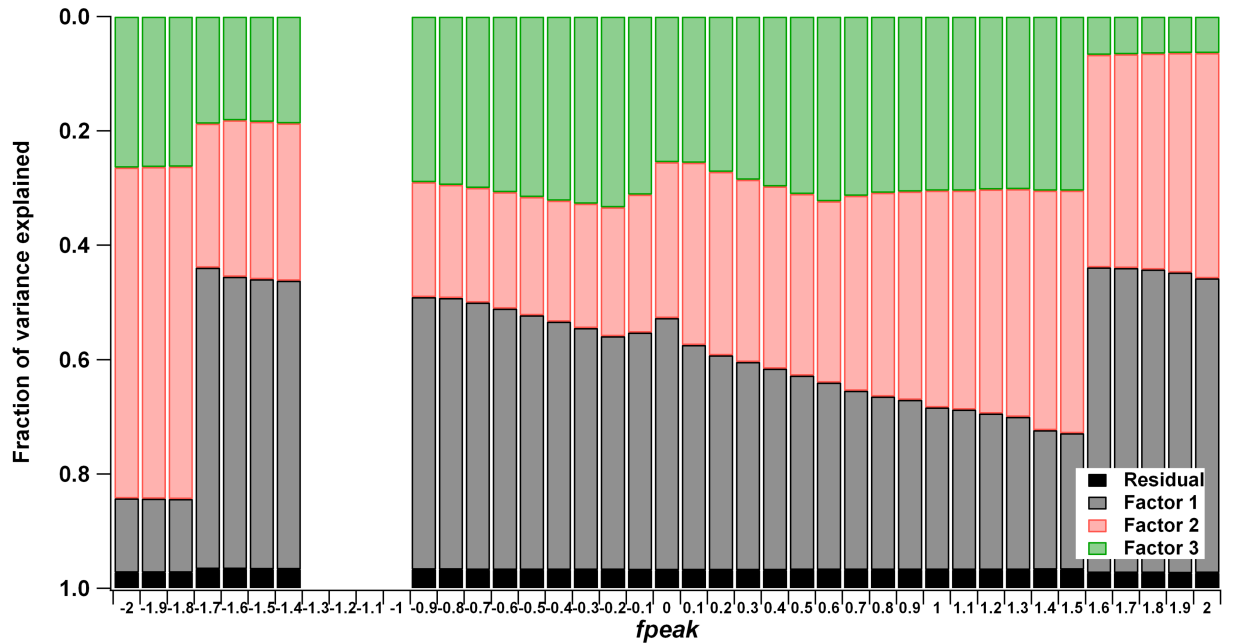
103
104



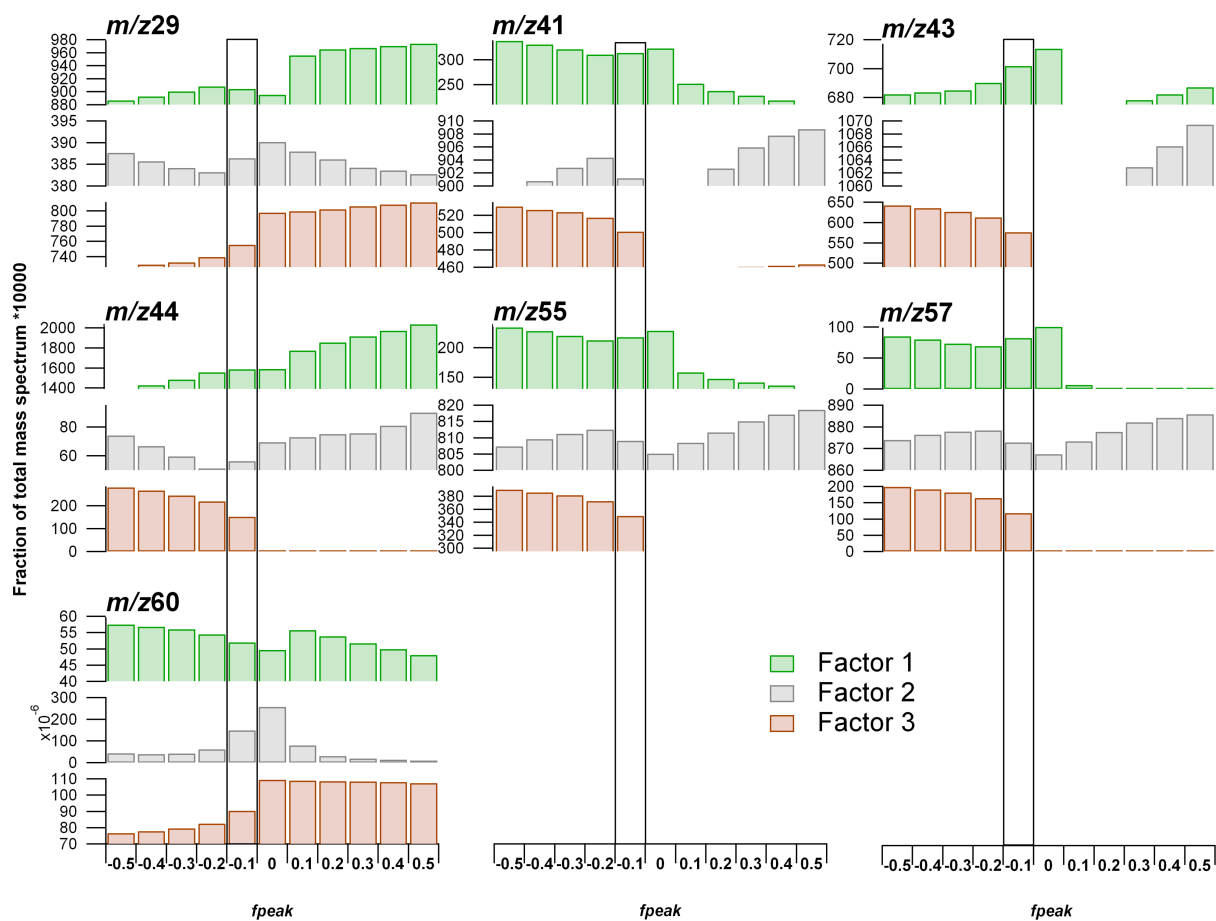
105
106 **Figure SI- 6: Q/Q_{exp} and the maximum value of the rotational matrix versus the number of factors for part 1**
107 **and part 2. The chosen solution is denoted by the orange circle.**
108



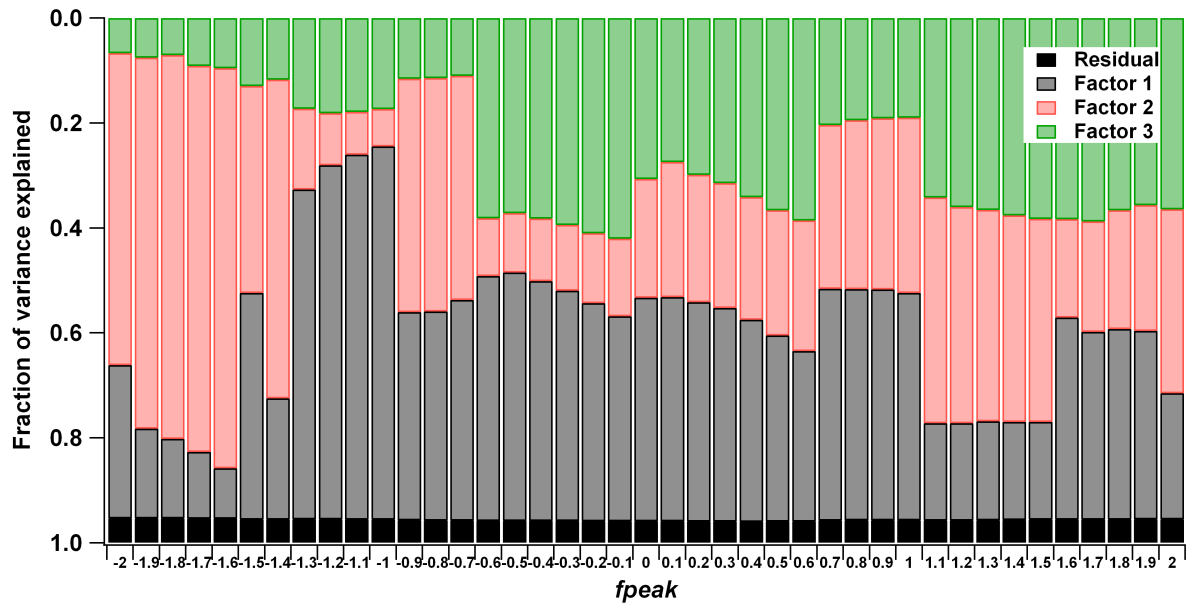
109
 110 Figure SI- 7: Q/Q_{exp} and the maximum value of the rotational matrix versus f_{peak} for part 1 and part 2. The
 111 chosen solution is denoted by the orange circle.
 112



113
 114 Figure SI- 8: Part 1 (data from 27 November 2007 – 19 February 2008) - variance explained by $p = 3$ as a
 115 function of rotational parameter f_{peak} . f_{peak} was chosen to be -0.1 for this part of the campaign.
 116

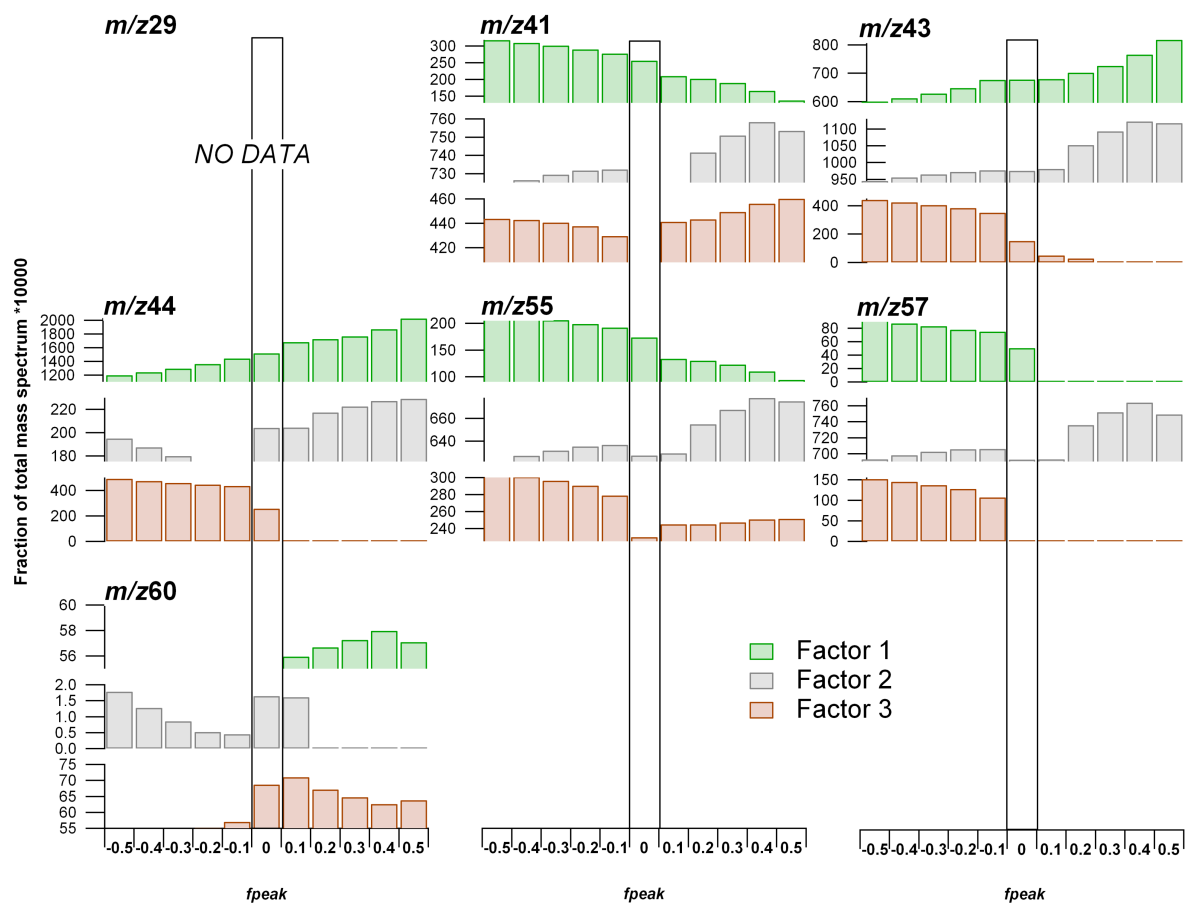


117
 118 Figure SI- 9: Part 1 (data from 27 November 2007 – 19 February 2008) - fraction of organic m/z 's 29 (CHO^+ ,
 119 C_2H_5^+), 41 (pre-dominantly C_3H_5^+), 43 ($\text{C}_2\text{H}_3\text{O}^+$, C_3H_7^+), 44 (pre-dominantly CO_2^+ , also $\text{C}_2\text{H}_4\text{O}^+$, C_2H_8^+), 55
 120 (pre-dominantly C_4H_7^+), 57 ($\text{C}_3\text{H}_5\text{O}^+$, C_4H_9^+), and 60 ($\text{C}_2\text{H}_4\text{O}_2^+$) as a function of f_{peak} [-0.5,0.5] for the 3-
 121 factorial solution. Note the different scaling of the y-axes. The boxes frame the chosen f_{peak} of -0.1.



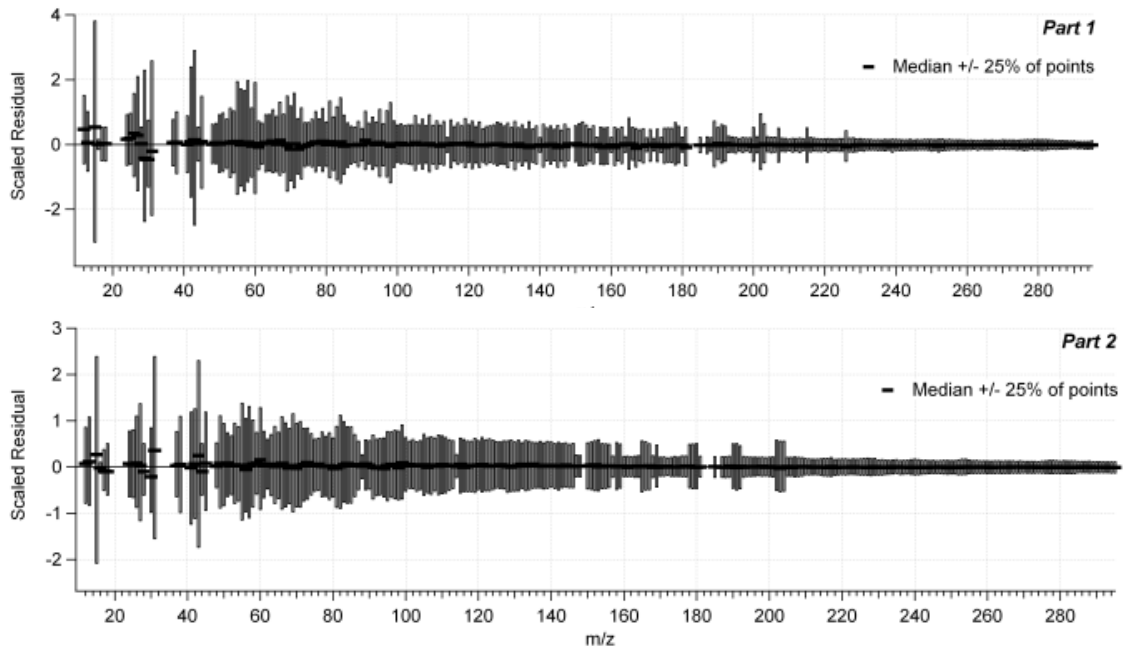
122
 123
 124
 125
 126

Figure SI- 10 Part 2 (data from 14 December 2008 – 16 December 2008) - variance explained by $p = 3$ as a function of rotational parameter f_{peak} . f_{peak} was chosen to be 0 for this part of the campaign.



127
 128 **Figure SI- 11: Part 2 (data from 14 December 2008 – 16 December 2008) - fraction of organic m/z 's 41 (pre-**
 129 **dominantly $C_3H_5^+$), 43 ($C_2H_3O^+$, $C_3H_7^+$), 44 (pre-dominantly CO_2^+ , also $C_2H_4O^+$, $C_2H_8^+$), 55 (pre-dominantly**
 130 **$C_4H_7^+$), 57 ($C_3H_5O^+$, $C_4H_9^+$), and 60 ($C_2H_4O_2^+$) as a function of f_{peak} [-0.5,0.5] for the 3-factorial solution. Note**
 131 **the different scaling of the y-axes. The boxes frame the chosen f_{peak} of 0.**
 132

133

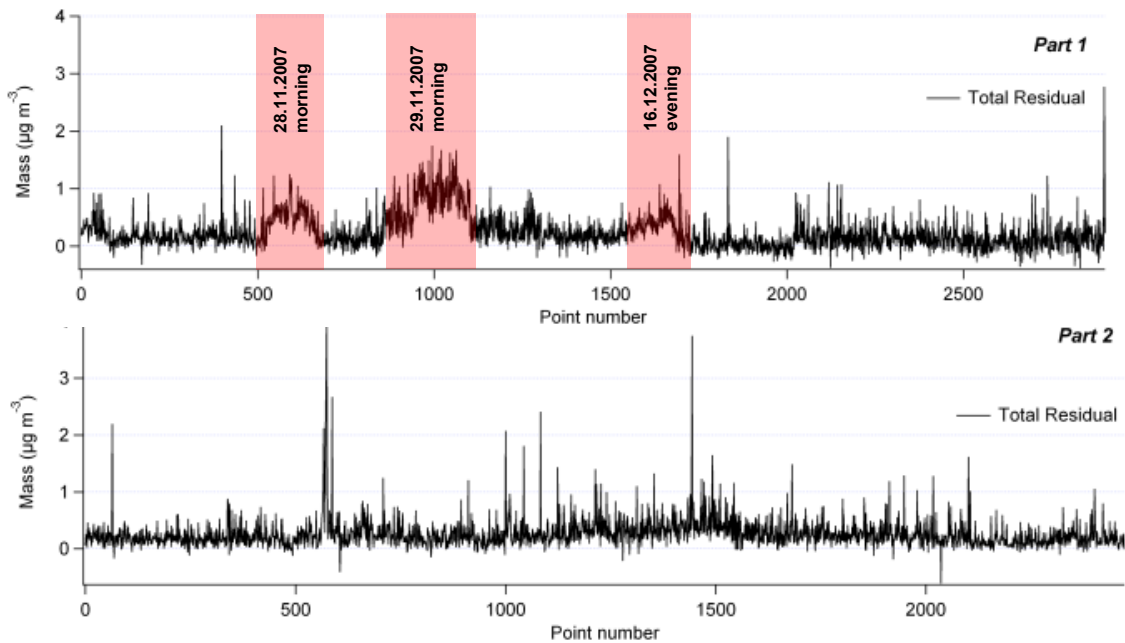


134

135 **Figure SI- 12: Boxplots of scaled residuals (only median and 25%-percentiles shown) as a function of m/z .**

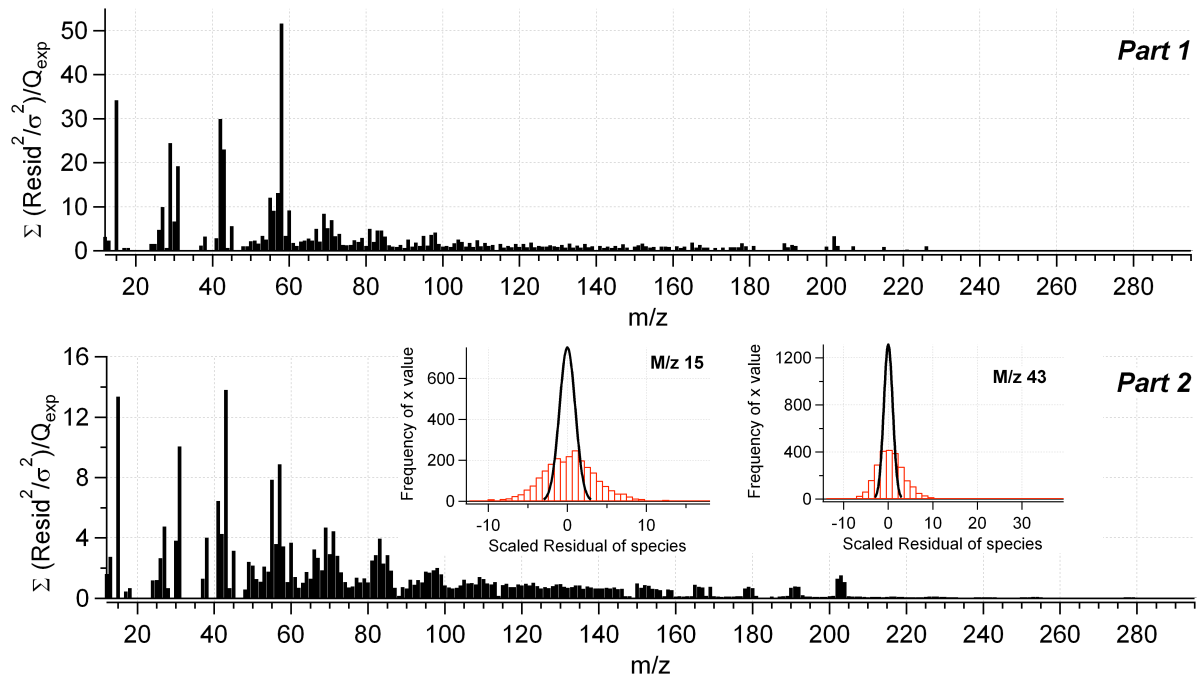
136

137



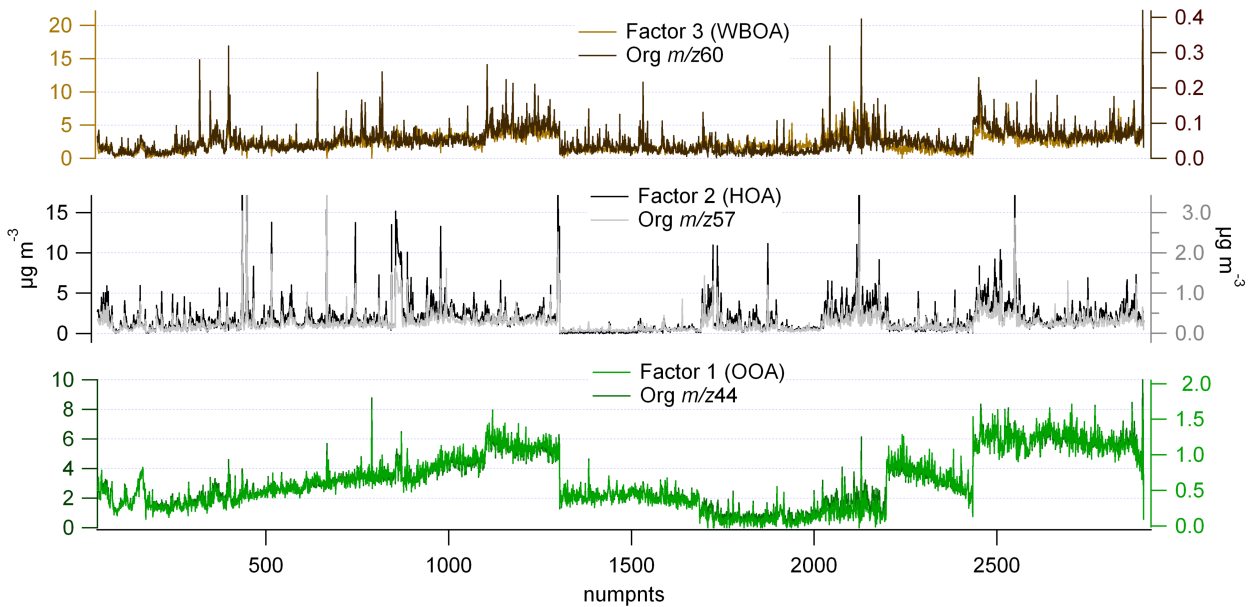
138

139 **Figure SI- 13: Time series of summed total residuals. Red bars in part 1 panel denote periods influenced by**
140 **amine-like factor.**



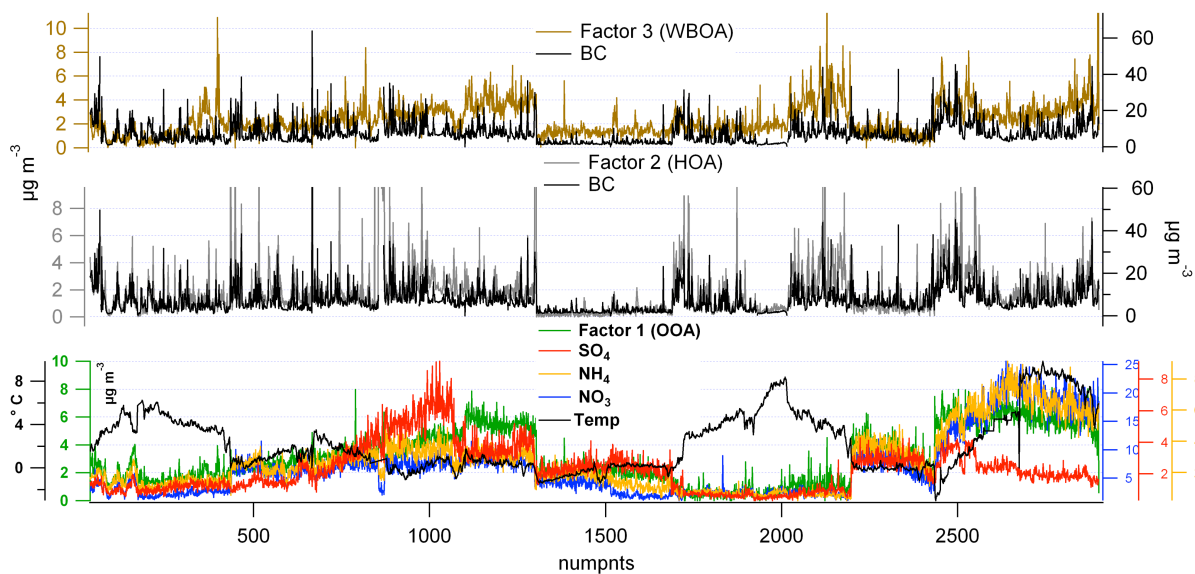
141
 142 **Figure SI- 14: Q/Q_{exp} as a function of m/z . Insets show normal distribution of scaled residuals for individual**
 143 **peaks. Note positive bias of distribution of residuals of m/z 58 for part 1.**

144
 145



146
 147 **Figure SI- 15: Part 1 – time series of factors and organic marker masses 60, 57, 44.**

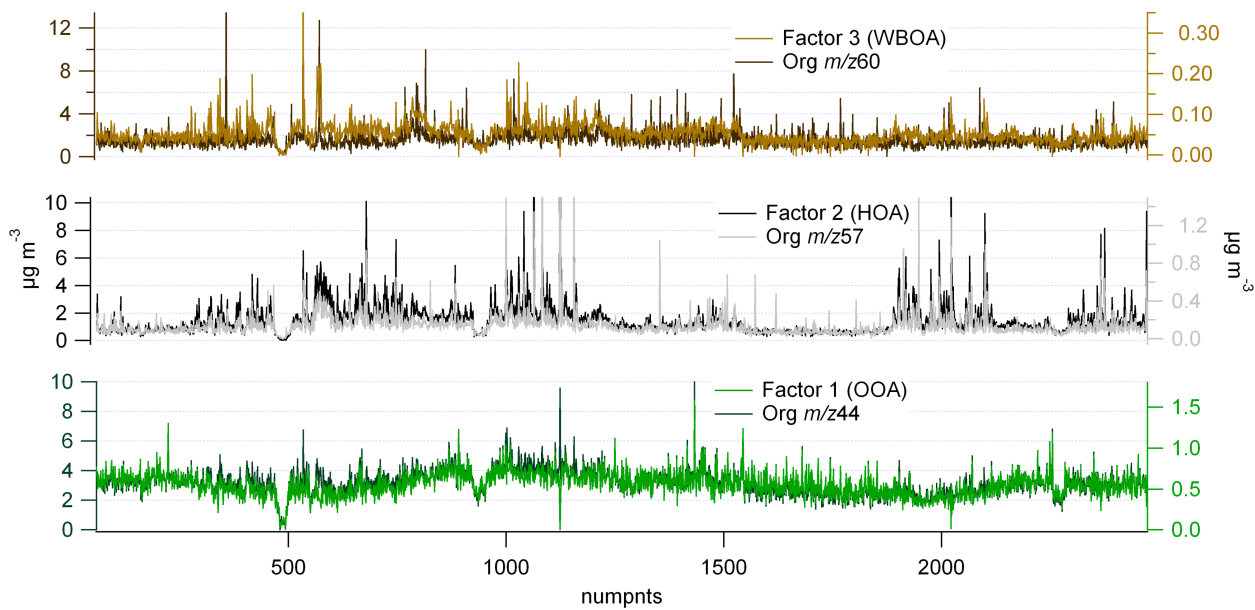
148



149

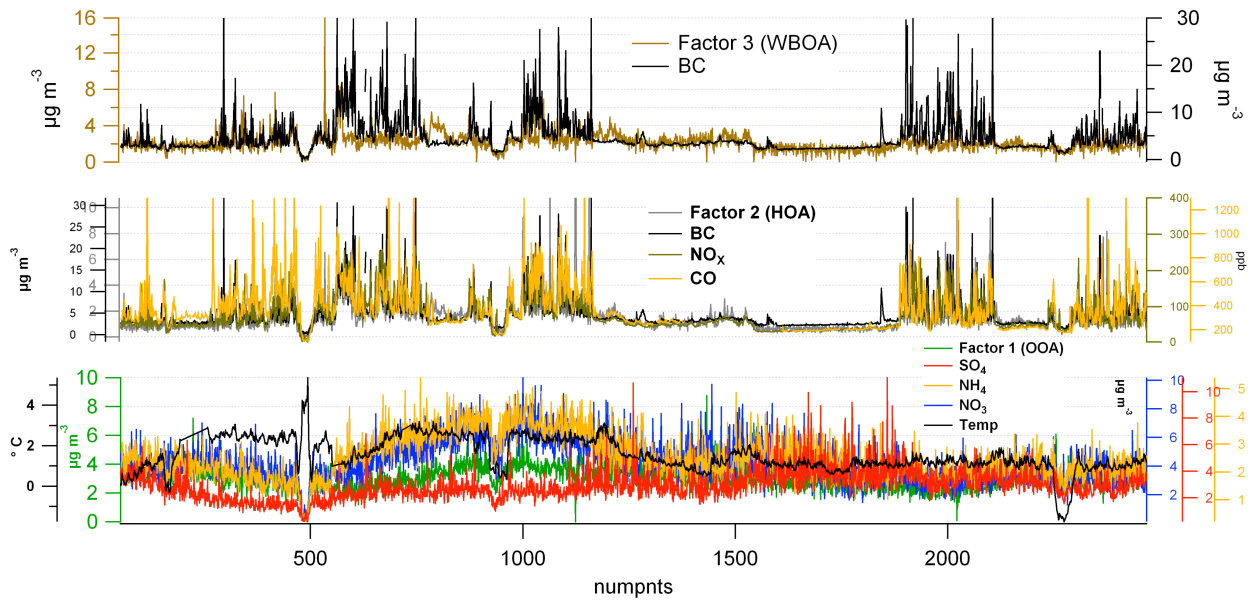
150 **Figure SI- 16: Part 1 – time series of factors and ancillary data.**

151



152

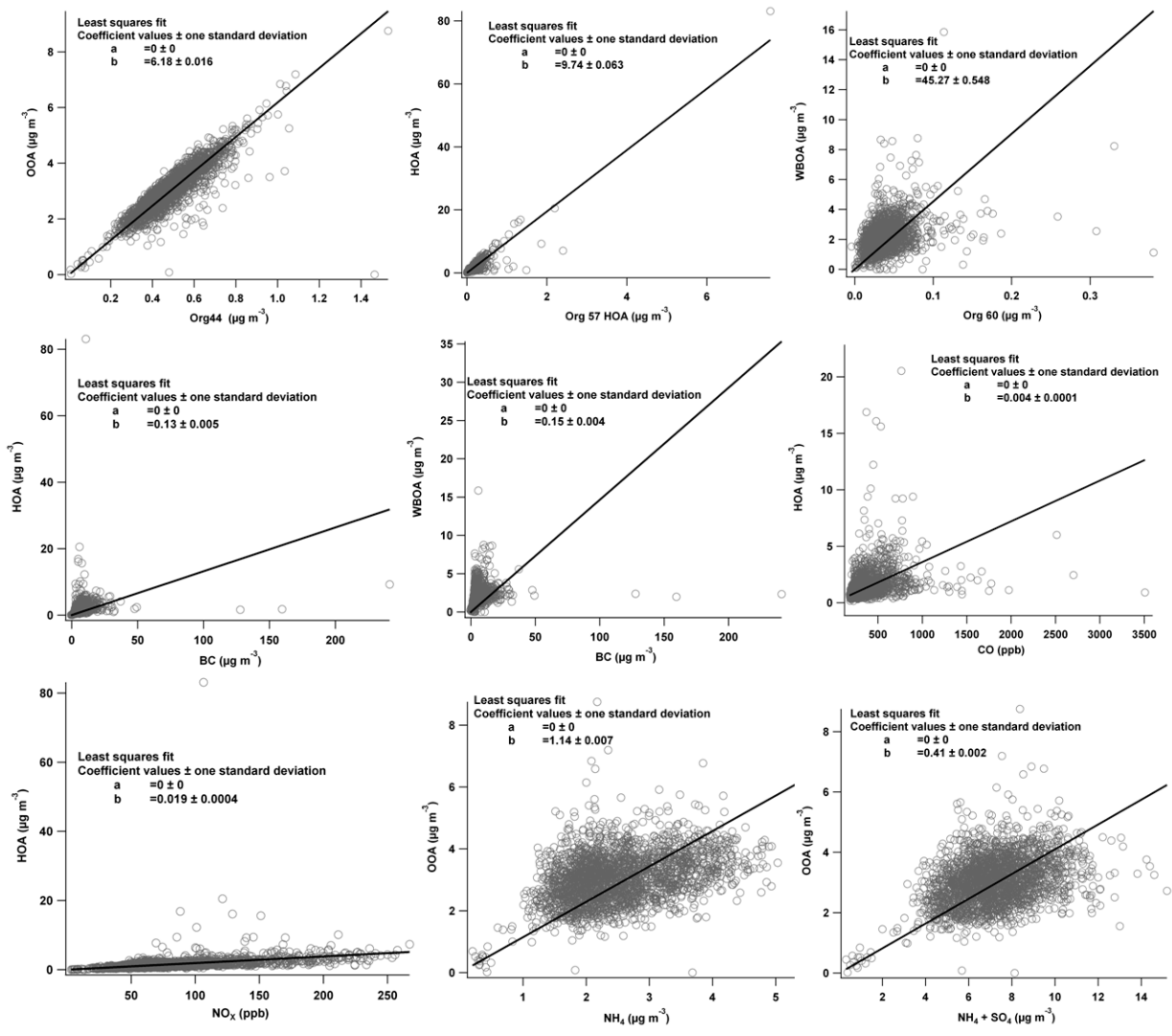
153 **Figure SI- 17: Part 2 - time series of factors and organic marker masses 60, 57, 44.**



154

155 **Figure SI- 18: Part 2 - series of factors and ancillary data.**

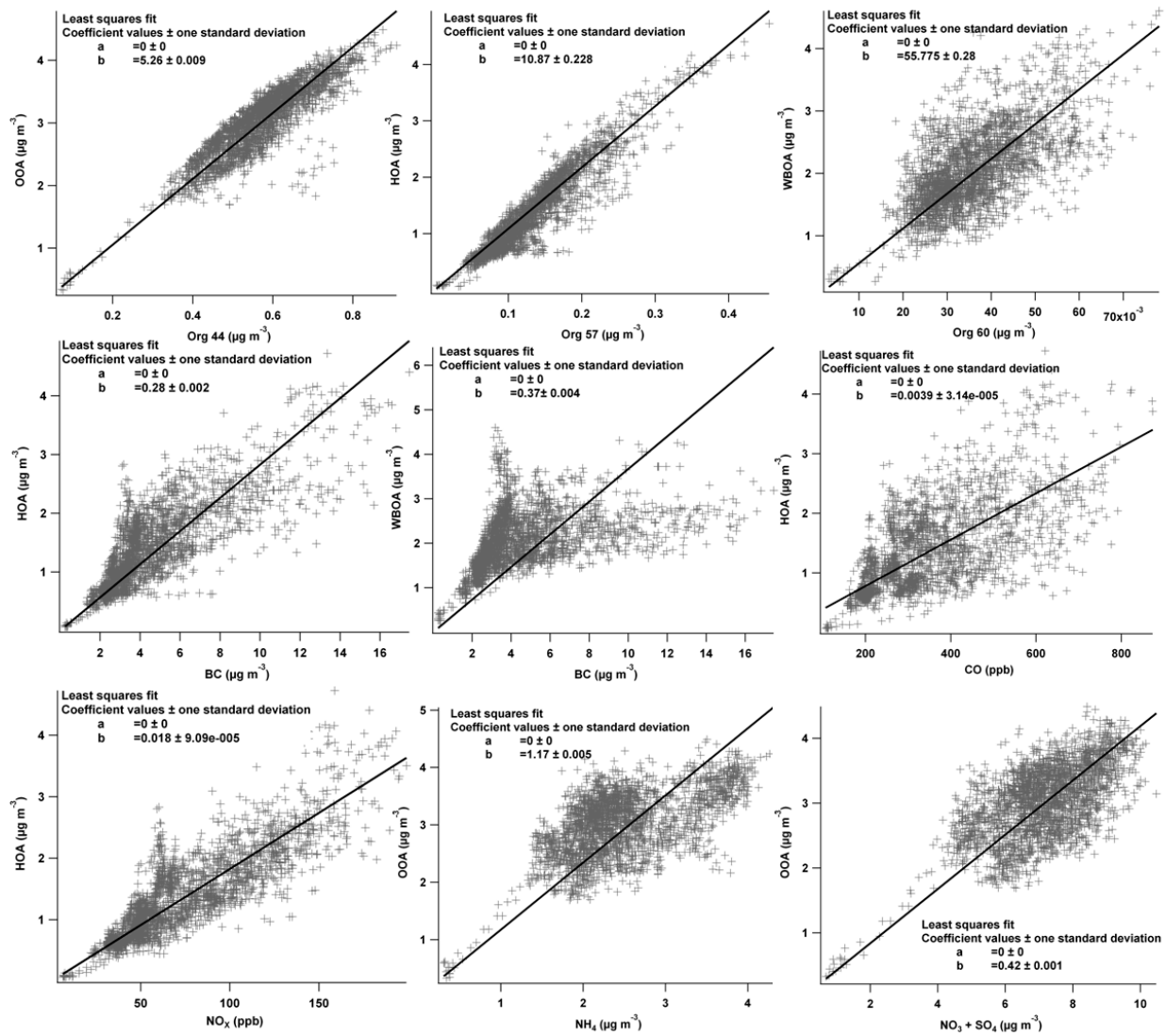
156



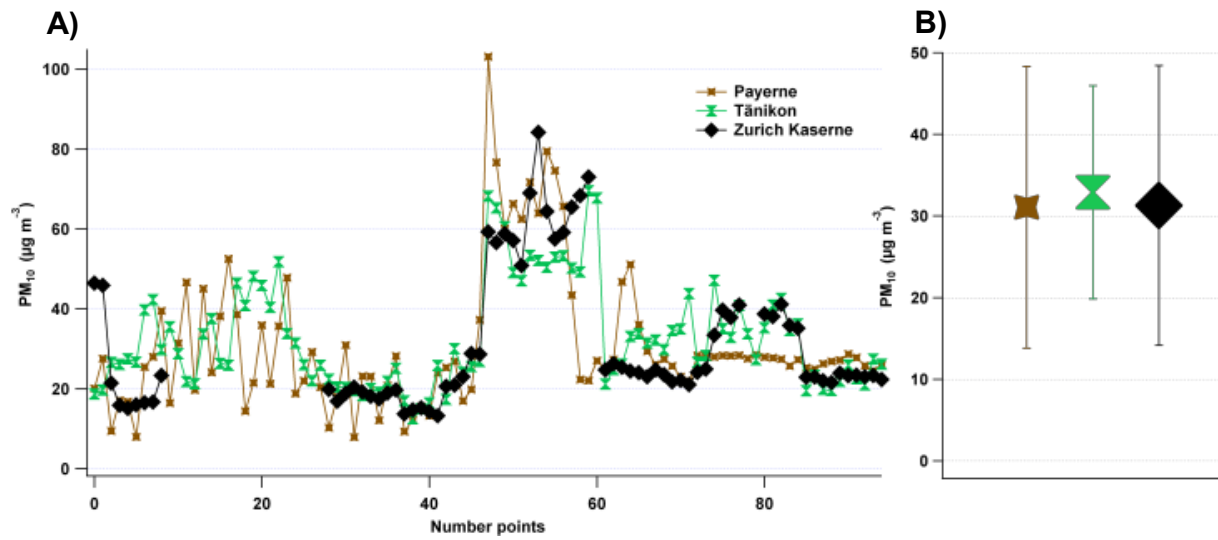
157

158

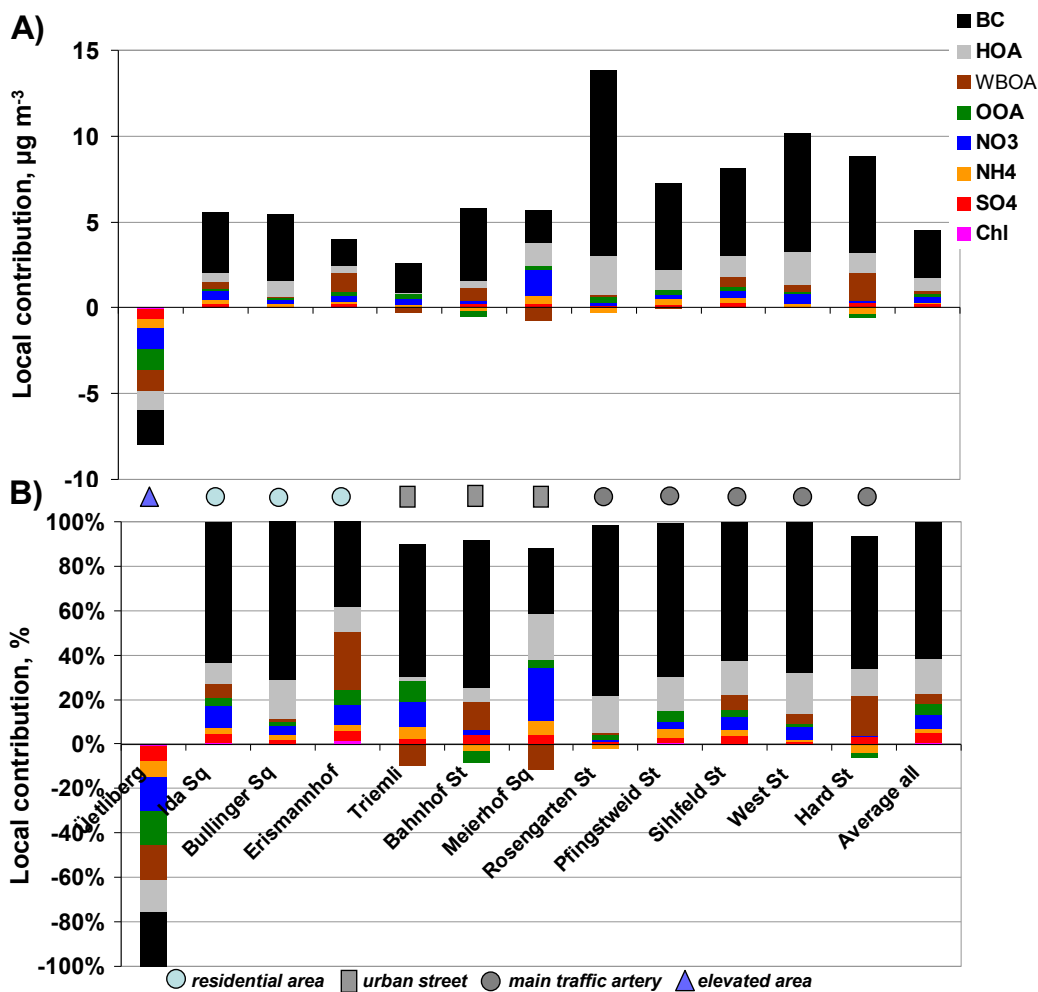
Figure SI- 19: Regression analysis of PMF factor time series and ancillary data, no corrections applied.



159
 160 **Figure SI- 20: Regression analysis of PMF factor time series and ancillary data, after removing the upper 1st**
 161 **percentile of data points and applying a moving average over 5 data points.**



163
164 **Figure SI- 21: Time series of PM₁₀ at Payerne (rural station), Tänikon (rural station), and Zurich Kaserne**
165 **(urban background station) (panel A) during the same time intervals as the mobile measurements. Panel B**
166 **shows the mean value and standard deviation of the time series in panel A.**



167
 168 **Figure SI- 22: Local concentrations calculated by subtracting the concentration of component S measured at**
 169 **Kaserne from the concentration of component S measured on-road at the same time (panel A, relative values**
 170 **panel B). For the time series of Kaserne data, the interpolated median value of 2 subsequent Kaserne visits**
 171 **was used. The “average all” bar is the mean value of the local contribution of all data.**

172
 173

174 **References**

175 Alfarra, M. R., Prevot, A. S. H., Szidat, S., Sandradewi, J., Weimer, S., Lanz, V. A., Schreiber,
 176 D., Mohr, M., and Baltensperger, U.: Identification of the mass spectral signature of organic
 177 aerosols from wood burning emissions, *Environ. Sci. Technol.*, 41, 5770 - 5777, 2007.

178 Fay, B., Glaab, H., Jacobsen, I., and Schrodin, R.: Evaluation of Eulerian and Lagrangian
 179 atmospheric transport models at the Deutscher-Wetterdienst using Anatex surface tracer data,
 180 *Atmos. Environ.*, 29, 2485-2497, 1995.

- 181 Koebel, M., Elsener, M., and Kleemann, M.: Urea-SCR: a promising technique to reduce NO_x
182 emissions from automotive diesel engines, *Catal. Today*, 59, 335-345, 2000.
- 183 Lanz, V. A., Alfarra, M. R., Baltensperger, U., Buchmann, B., Hueglin, C., and Prevot, A. S. H.:
184 Source apportionment of submicron organic aerosols at an urban site by factor analytical
185 modelling of aerosol mass spectra, *Atmos. Chem. Phys.*, 7, 1503-1522, 2007.
- 186 Paatero, P., Hopke, P. K., Song, X. H., and Ramadan, Z.: Understanding and controlling rotations
187 in factor analytic models, *Chemometr. Intell. Lab.*, 60, 253-264, 2002.
- 188 Silva, P. J., Erupe, M. E., Price, D., Elias, J., Malloy, Q. G. J., Li, Q., Warren, B., and Cocker, D.
189 R.: Trimethylamine as precursor to secondary organic aerosol formation via nitrate radical
190 reaction in the atmosphere, *Environ. Sci. Technol.*, 42, 4689-4696, 10.1021/es703016v, 2008.
191
192